LUND UNIVERSITY

Noncollinear Magnetism

Hobbs, David; Hafner, Jürgen

Published in:
Annals of the Marie Curie Fellowship Association

2006

Link to publication

Citation for published version (APA):
Hobbs, D., & Hafner, J. (2006). Noncollinear Magnetism. *Annals of the Marie Curie Fellowship Association*, *4*, 1-6.

Total number of authors:
2

General rights
Unless other specific re-use rights are stated the following general rights apply:
Copyright and moral rights for the publications made accessible in the public portal are retained by the authors and/or other copyright owners and it is a condition of accessing publications that users recognise and abide by the legal requirements associated with these rights.
• Users may download and print one copy of any publication from the public portal for the purpose of private study or research.
• You may not further distribute the material or use it for any profit-making activity or commercial gain
• You may freely distribute the URL identifying the publication in the public portal

Read more about Creative commons licenses: https://creativecommons.org/licenses/

Take down policy
If you believe that this document breaches copyright please contact us providing details, and we will remove access to the work immediately and investigate your claim.

LUND UNIVERSITY

PO Box 117
221 00 Lund
+46 46-222 00 00

Noncollinear Magnetism

David Hobbs[1] (hobbs@tele2adsl.dk) and Jürgen Hafner[2] (juergen.hafner@univie.ac.at)
[1]Terma A/S, Space, Vasekær 12, 2730 Herlev, Denmark
[2]Institut für Materialphysik, Sensengasse 8/12, A-1090 Wien, Austria

Abstract

Recently, a great deal of effort has been focused on developing the so called "fully unconstrained" approach to noncollinear magnetism. This approach allows the magnetization density within a material to be calculated as a continuous vector variable of position, as opposed to using the atomic moment approximation (AMA) where a fixed quantization direction is assumed for a volume-filling sphere surrounding each atomic site, i.e., the constrained approach. In this paper a number of applications of the method are reviewed. Initially, only small clusters of Iron (Fe) and Chromium (Cr) atoms were studied which nicely illustrated some possible noncollinear magnetic arrangements. However, later research has been applied to triangular free-standing Cr and Manganese (Mn) monolayers and overlayers on Cu substrates. Finally, noncollinear magnetism has been investigated within the different phases of Mn, including the complex α-Mn phase, which has been shown experimentally to have a noncollinear magnetic structure.

1 INTRODUCTION

1.1 Related Studies

The motivation for a fully unconstrained approach is to allow the magnetization density to be correctly treated in the interstitial regions between atomic sites. While many materials have well localized magnetization densities for which the AMA is valid, others may exhibit a de-localized magnetization density, which is more appropriately treated with a fully unconstrained approach. Oda *et al.* [1] were the first to implement such an approach within a plane-wave pseudopotential scheme. Both the atomic and magnetic structures were allowed to relax simultaneously and self-consistently. Ivanov and Antropov [2] developed a wavelet technique for calculating the electronic and noncollinear magnetic structures in the framework of spin-density functional theory, again without imposing shape restrictions on the magnetization density by studying the spin-structures of H_3 and Cr_3 clusters.

In parallel with our efforts, Nordström and Singh [3], and Asada *et al.* [4] have concentrated on developing the method within the full-potential linearized augmented plane-wave (FLAPW) formalism. The approach of Nordström and Singh [3] is fully unconstrained in the sense discussed above, while that of Asada *et al.* [4] is adapted to suit the film geometry for surfaces and open structures. This adaptation imposes a constraint. The magnetization density is treated as a continuous vector field in the interstitial region and in a vacuum, while inside each muffin-tin sphere they allow only a fixed spin quantization axes. Since in the FLAPW the muffin-tin spheres are significantly smaller than the volume filling atomic spheres, this extra constraint is a reasonable one.

1.2 Origins of Noncollinear Magnetism

A large number of compounds exhibit magnetic behavior. This can be ferromagnetic (FM), where spins are aligned in parallel directions, anti-ferromagnetic (AFM), where the spins are anti-parallel, or noncollinear, where the spins are not parallel and may be disordered. Often, Mn is one of the elements in these compounds. Although it not perfectly understood why, Mn lies in the middle of the transition metal series and can have competing FM and AFM interatomic exchange interactions lying between those of the early transitions metals, which are largely AFM, and those of the late transition metals, which are largely FM. Examples of competing exchange interactions include disordered systems such as topological glasses, spin-glasses and substitutional alloys.

Noncollinear magnetism can also arise naturally due to geometric frustration of AFM interactions. For example, in an equilateral triangular structure with atoms at each apex the frustrated spins have a 120º angle between them, if we assume a Heisenberg model with equal exchange interactions. Such triangular arrangements can exist in real solids and, as we shall see later, the α- and β- phases of Mn have an atomic structure that contains triangular planes. Thus, we can expect noncollinear magnetic structures to arise from geometric frustration.

Other effects giving rise to noncollinear magnetism include magnetic anisotropy, which arises due to a preferred direction of magnetization. There are several different types of anisotropy:

- Magnetocrystalline which results from interactions of the spin magnetic moments with the crystal lattice. This relativistic effect enters via spin-orbit coupling and is strongly dependent on the crystal symmetry.
- Surface due to broken symmetry at the surface.
- Stress which is induced on the crystal structure due to magnetization, and vice versa.
- Shape due to the shape of individual mineral grains.

Magnetic anisotropy strongly affects the shape of the material's hysteresis loop and is also of practical importance because it is exploited in the design of most magnetic materials of commercial importance. Finally,

competition between exchange interactions and magnetic anisotropy also contribute to noncollinear magnetism.

2 THE NONCOLLINEAR FORMALISM

2.1 Theory of Noncollinear Magnetism

A generalization of von Barth and Hedin's [5] local spin-density functional (LSDF) theory to noncollinear magnetism was first proposed by Kübler *et al.* [6] within the framework of the augmented-spherical-wave (ASW) method and the atomic-sphere approximation. The effective single particle equations for noncollinear magnets were derived by allowing the spin-quantization axis to vary from site to site in crystalline systems. The orientation of the axis with respect to the reference frame is a property of the ground state. They predicted well-defined sets of directions for the spins, which are uncoupled from the crystal lattice unless spin-orbit coupling effects are included in the Hamiltonian (even though such effects are small in comparison to the spin–spin interactions).

The spin-polarized density functional theory is expressed in terms of a 2×2 density matrix with elements $n^{\alpha\beta}(\vec{r})$. The electron density is then:

$$Tr\left[n^{\alpha\beta}(\vec{r})\right] \equiv n_{Tr}(\vec{r}) = \sum_{\alpha} n^{\alpha\alpha}(\vec{r})$$

The total-density matrix may then be defined as:

$$n^{\alpha\beta}(\vec{r}) = \left(n_{Tr}(\vec{r})\delta_{\alpha\beta} + \vec{m}(\vec{r}) \cdot \vec{\sigma}^{\alpha\beta}\right)/2$$

In addition, for the density matrix, we can make a transformation to the equivalent magnetization density using the following formula:

$$\vec{m}(\vec{r}) = \frac{e\hbar}{mc} \sum_{\alpha\beta} n^{\alpha\beta}(\vec{r}) \cdot \vec{\sigma}^{\alpha\beta}$$

where $\vec{\sigma} = (\sigma_x, \sigma_y, \sigma_z)$ are the Pauli spin matrices. As the electron density becomes a 2×2 density matrix in the noncollinear spin-polarized theory this leads to a significant increase in the computational effort.

2.2 Projector-Augmented-Wave Method

The fully unconstrained method has been developed within the all-electron projector augmented-wave (PAW) method, which is based on the generalized local spin density theory. This method allows both the atomic and magnetic structures to relax simultaneously and self-consistently. The algorithms have been implemented within a powerful and widely used package called VASP (Vienna *ab-initio* simulation package), which has been used successfully for a large variety of different systems such as crystalline and amorphous semiconductors, simple liquids and transitional metals.

The PAW method is an all-electron method for electronic structure, total-energy, and force calculations, which is closely related to the ultrasoft-pseudopotential technique. In the PAW approach, charge and spin densities are decomposed into pseudo-densities and compensation densities accounting for the difference between the pseudo-densities and all-electron densities. The pseudo-densities consist of a smooth part expressed in a plane-wave representation, and localized augmentation charges accounting for the violation of norm conservation. Both augmentation and compensation charges are represented on radial support grids. For each of the atom-centered radial support grids the spin-quantization axis is fixed and, in this respect, our approach resembles the unconstrained non-collinear FLAPW technique, but unlike the FLAPW method, in the PAW approach the plane-wave description is not restricted to the interstitial region, but extends over the complete volume of the system. Hence, variations of the magnetization direction are allowed also within the augmentation spheres. For further details of the non-collinear PAW formalism we refer to Hobbs *et al.* [7].

3 APPLICATIONS

3.1 Magnetic Properties of Fe and Cr

Small clusters of Fe_n (n<5) have been studied extensively in the past and represent ideal systems for testing our implementation of noncollinear magnetism. As fcc Fe is known to have a spin-spiral ground-state, noncollinear magnetism is suspected to be important in Fe clusters, largely as they have less symmetry constraints than bulk materials. In addition to Fe, we have also investigated the ground states of Cr_n (n<5) clusters. For crystalline Fe and Cr it has been shown that the local-density-approximation (LDA) leads to incorrect predictions of the structural and magnetic ground state, e.g., Fe is predicted to be hexagonal-close-packed and nonmagnetic (NM) instead of body-centered-cubic and FM. The LDA also fails in assessing the strength of the magneto-volume effect. The generalized gradient approximation (GGA) contains non-local corrections to the exchange-correlation functionals, which depend on the absolute values of the gradients of charge and spin density, and leads to a correct prediction of the structural and magnetic phase diagram. As examples of noncollinear magnetic arrangements in Fe we focus on the Fe_3 linear chain and an Fe_5 bipyramidal. For Cr, examples include a Cr_3 triangular structure, which we shall see in the next section is important in the context of triangular layer structures, and the Cr_4 pyramidal structure. The full details of our cluster studies can be found in Hobbs *et al.* [7].

For Fe_3 we considered an equilateral triangle and a linear chain. For the triangular structure a collinear FM state was found to be the ground state with a magnetic moment of ~2.97 μ_B/atom. However, the linear chain, while not the ground state for Fe_3 clusters, is of particular interest as Oda *et al.* [1] have reported noncollinear magnetic arrangements for this structure using a plane wave pseudopotential scheme. In contrast, all our results are collinear even when we initiate a noncollinear

arrangement similar to the ground state found by them. Interestingly, during these calculations we found such noncollinear arrangements, but when the accuracy was increased to obtain full convergence, a magnetic phase transition occurs, reducing the total energy, to give a collinear result. This metastable noncollinear state is illustrated in Figure 1 together with the Fe_5 solution. For Fe_5, a noncollinear ground state is found for a bipyramidal structure which has a roughly FM ground state but also contains tilted magnetic moments on the apical atoms of the bipyramid. Intuitively such solutions seem to be unphysical as they break the normal collinear symmetry and one would expect the total energy to be higher. Nevertheless, in both GGA and LDA we have been able to stabilize such solutions some 14 meV/atom and 32 meV/atom below the collinear results, respectively. How such frustration might arise is not immediately clear. The coupling between the apical atoms must play a crucial role in establishing the frustration. As the moments on the apical atoms tilt in opposite directions, it appears that the exchange interactions between the apical atoms are AFM and, hence, act against the FM nearest neighbor coupling between apical and central atoms. Hence, a rotation of the apical moments relative to those in the central triangle allows the magnetic energy to be optimized.

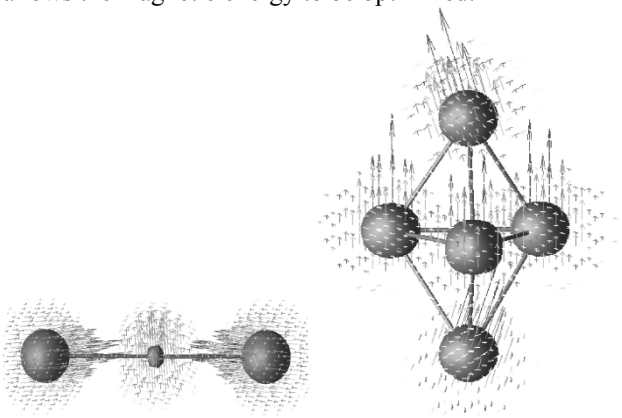

Figure 1 : Three dimensional views of the magnetization density for metastable Fe_3 atoms in a linear chain and a stable Fe_5 bipyramidal structure.

For triangular Cr_3 clusters the ground state was found to be a ferrimagnetic distorted triangular structure. In addition, we have also found a metastable ‘‘spiral’’ arrangement, which is illustrated in Figure 2 together with a stable noncollinear solution for Cr_4. In this case the Cr_3 triangular structure is undistorted. The figure illustrates that this solution corresponds to the classical frustrated AFM trimer. The Cr ions have rather localized magnetic moments and the transition from one direction of magnetization to another goes through zero magnetization at the ‘‘Bloch wall’’ rather than through a rotation of magnetization. Cr_4 is interesting in terms of noncollinear arrangements of the magnetic moments. We find three solutions: a metastable FM with small bulk-like moments, a noncollinear metastable state, which is a generalization of the spiral arrangement found in Cr_3 with the magnetization directions on the neighboring atoms forming a tetrahedral angle of 109.5°, and an AFM ground state. In the noncollinear case the total atomic magnetic moment is 4.02 μ_B/atom using GGA and is symmetric on all sites. To summarize, the figures presented here illustrate, firstly, that the magnetization density varies smoothly with position; secondly, that the spin direction only changes at the ‘‘Bloch wall’’ between atoms where the charge and spin densities are small; and thirdly, that the magnetization density is roughly uniform in the magnetic region of the atoms. This justifies the use of the atomic-sphere approximation applied to materials with strong atomic magnetization.

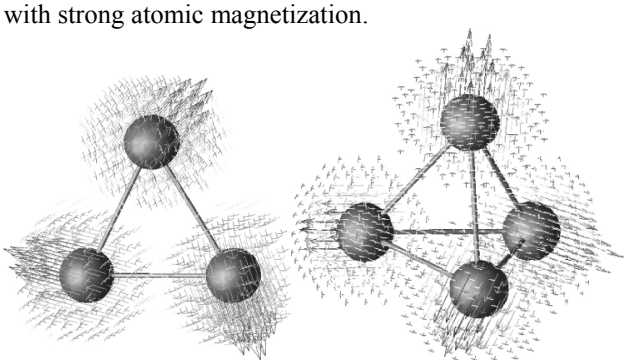

Figure 2 : The metastable magnetization density for Cr_3 in a triangular structure and a Cr_4 pyramidal structure.

3.1 Triangular Cr and Mn Layers

Subsequent to demonstrating the potential of this method, it has also been applied to study the magnetic ground state of triangular free-standing Cr and Mn monolayers and overlayers on Copper (Cu) substrates [8]. Such systems represent a physical realization of a frustrated two-dimensional antiferromagnet. Previous calculations of this type neglected the fact that the magnetic configuration can break the symmetry of the surface. In our study of small magnetic clusters, we found that for triangular Fe3 and Cr3 clusters the expected result, that the magnetic ground state is non-collinear, is circumvented because the structure relaxes away from the equilateral triangle, thus allowing a collinear AFM ground state to be formed. The present calculations consider:

- the FM p(1×1) structure with one surface atom in the two-dimensional unit cell,
- the collinear row-wise AFM structure with c(2×2) periodicity and two atoms in the unit cell,
- the non-collinear 120º configuration of nearest neighbor magnetic moments with a $\left(\sqrt{3}\times\sqrt{3}\right)R30°$ unit cell containing three surface atoms.

Figure 3 shows the latter structure. Unlike the planar FM model, where only global spin-rotation symmetry is broken, an additional reflection symmetry is broken in this case. The figure indicates two topologically distinct patterns, characterized by different helicities. Each elementary triangle is assigned a helicity according to the way the three spins at the vertices of the triangle are aligned. A positive helicity describes an arrangement in which the spins are rotated sequentially by 120º clockwise

when the triangle is traversed in a clockwise direction, while a negative helicity refers to anticlockwise rotations traversing the triangle in a clockwise direction. In the following we shall first discuss the properties of free-standing monolayers.

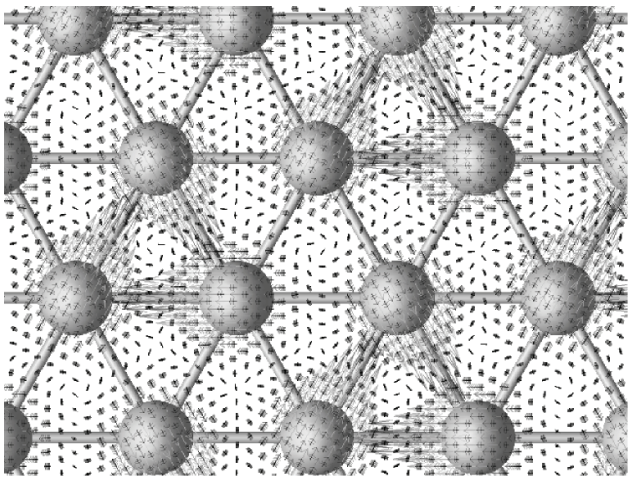

Figure 3 : Noncollinear magnetic structure of a triangular Cr layer on Cu(111) with the magnetization density superimposed.

Figure 4 summarizes our results for the magnetic moments and total energies of the three possible magnetic configurations as a function of the nearest-neighbor bond-length. In both Cr and Mn monolayers, a FM high-spin phase with a magnetic moment of nearly 4 μ_B is stable only at expanded interatomic distances. In Cr monolayers the magnetic moment breaks down rather suddenly at a bond-length of about 2.57 Å, the FM minimum being about 280 meV higher in energy than the non-magnetic minimum. In Mn monolayers we find a transition from a FM high-spin phase at bond-lengths larger than 2.47 Å to a FM low-spin phase at closer interatomic distances. The low-spin phase ($M \leq 1{:}5\ \mu_B$) loses its magnetic moment only at strongly reduced bond-lengths. The row-wise AFM c(2×2) Cr monolayer has an equilibrium bond-length of 2.70 Å at a magnetic moment of 3.75 μ_B. Under compression the magnetic moment is strongly reduced, disappearing at a bond length of 2.31 Å, corresponding roughly to the bond length of the NM phase.

The noncollinear 120º phase represents the magnetic ground state, and the equilibrium bond length is about 2.65 Å. At these distances, the magnetic moment is slightly smaller than in the AFM phase. Under compression, the noncollinear magnetic moments are gradually reduced. They disappear at distances somewhat smaller than the equilibrium distances in the NM phase. In Mn monolayers the relative stability of the AFM and noncollinear phase is reversed, the equilibrium bond lengths and magnetic moments being almost the same in both phases. Under compression, the magnetic energy difference is quickly reduced, at bond lengths smaller than about 2.35 Å, both phases are energetically almost degenerate. The AFM ground-state in Mn is somewhat surprising, - to investigate this point further we have also considered the same three configurations adsorbed on Cu(111) substrates. For comparison, the vertical lines in Figure 4 show the lateral lattice constant of the Cu(111) substrate. We find that triangular Mn-layers show an almost ideal epitaxial match to the substrate, whereas adsorbed Cr-layers undergo a small compressive strain. In both the AFM and the noncollinear phases, the magnetic moments are reduced compared to the freestanding monolayer. The important point is that for Mn/Cu(111) the AFM phase remains energetically favored. The different behavior of triangular layers of Cr and Mn is clearly related to the rather long-range nature of the exchange interactions in the Mn layers.

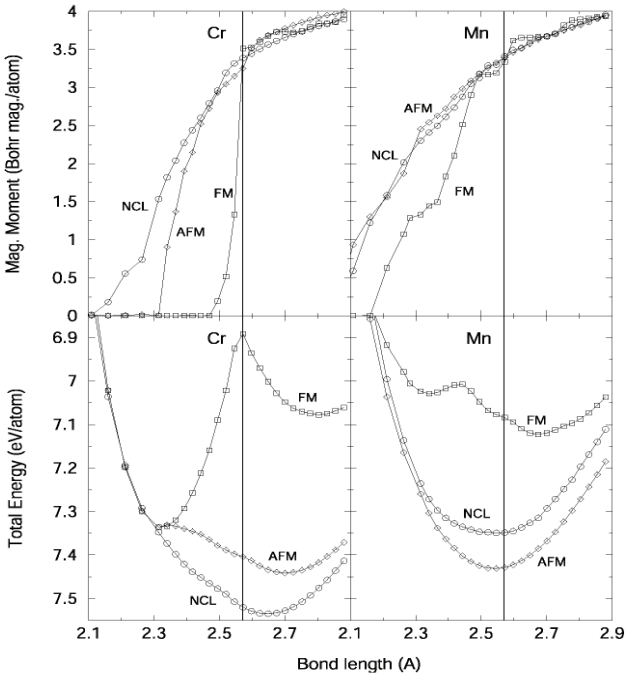

Figure 4 : Total energy and magnetic moments of the FM, the AFM, and the noncollinear phases of free-standing triangular Cr and Mn monolayers as functions of the nearest-neighbor bond length. The vertical lines mark the lateral interatomic distance of a Cu(111) substrate.

Figure 3 shows the magnetization density calculated for the noncollinear phase of Cr on Cu(111). The local direction of the magnetic moment is indicated by the arrows, the length of the arrows being proportional to the absolute value of the magnetization density. In addition, around each site iso-surfaces of the magnetization densities are drawn. At first glance, one tends to conclude that the magnetization densities are fairly well localized and, as the iso-surfaces are also almost spherical at reasonably large values, the conclusion that the AMA is a reasonable choice in this system seems to be appropriate. However, the regions around the atoms in which the direction of magnetization is approximately constant are distinctly smaller than the muffin-tin spheres of the FLAPW method or the overlapping atomic spheres of the LMTO approach. Interesting new aspects of this study are seen precisely in the bonding and interstitial regions where the direction of the magnetization changes.

3.2 Noncollinear Magnetism in α-Mn

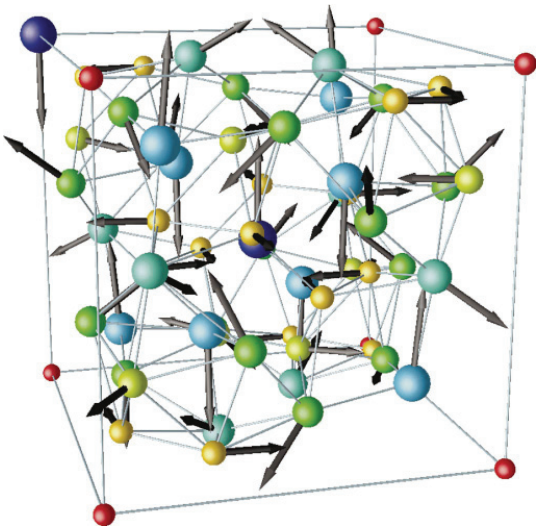

Figure 5 : Crystalline and magnetic structure of antiferromagnetic α-Mn. Atomic positions in the full cubic unit cell and magnitude and directions of the magnetic moments are shown. Atoms on crystallographically inequivalent sites are marked by different colors: dark blue: MnI, light blue: MnII, green and turquoise: MnIII (a) and (b), yellow and yellow-green: MnIV (a) and (b).

As an example of another application we review the different phases of Mn [9][10], which is an element with outstanding structural and magnetic properties. While most metallic elements adopt a simple crystalline structure and order magnetically - if at all - in a simple FM or AFM configuration, the stable phase of Mn, paramagnetic α-Mn, adopts a complex crystal structure with 58 atoms in the cubic cell. At a Neél[1] temperature of 95 K, a transition to a complex noncollinear AFM phase takes place. The magnetic phase transition is coupled to a tetragonal distortion of the crystalline structure. The strange properties of Mn arise from conflicting tendencies to simultaneously maximize the magnetic spin moment and the bond strength. Short interatomic distances produced by strong bonding tend to quench magnetism.

Figure 6 shows the total energy of paramagnetic and both collinear and noncollinear AFM α-Mn as a function of volume. Also shown is the variation of the magnitude of the magnetic moments on the crystallographically inequivalent sites. The magnetic structure is found to be strongly coupled to the crystal structure. The onset of magnetic ordering occurs at an atomic volume of about 9.5 Å, up to a volume of about 12 Å the magnetic structure remains collinear, with NM Mn atoms on sites IV. For larger atomic volumes, a metastable collinear magnetic configuration coexists with the stable noncollinear phase.

[1] The temperature at which ferrimagnetic and antiferromagnetic materials become paramagnetic

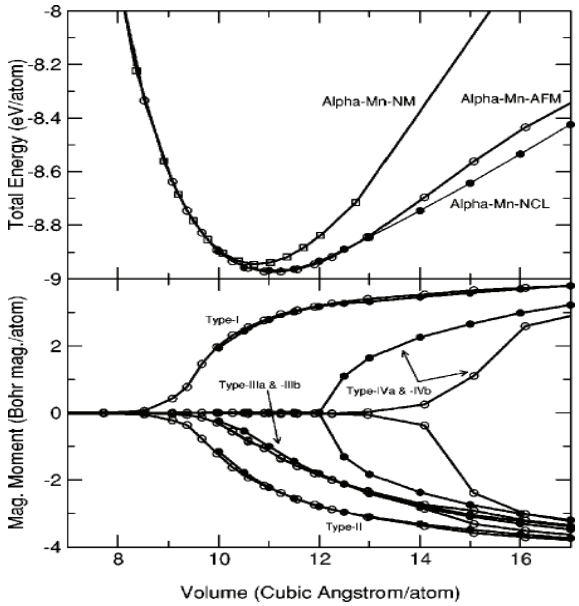

Figure 6 : Total energy of NM, collinear AFM and noncollinear AFM α-Mn as a function of volume. The absolute values of the calculated magnetic moments on the crystallographically inequivalent sites in noncollinear AFM α-Mn are also shown.

To find this noncollinear structure we started with a strongly expanded volume of 16 Å, and an experimental noncollinear magnetic structure but with artificially enhanced magnetic moments on the Mn IV sites. This calculation converged to a noncollinear minimum substantially lower in energy than the still metastable collinear structure. Noncollinear solutions at lower volumes could than be found by using a rescaled atomic and magnetic structure as the starting point for the optimization. As long as the Mn IV atoms are NM, the collinear AFM structure is only weakly frustrated. The coupling between Mn I and Mn II is AFM, and the frustration of the magnetic coupling in the triangular groups of Mn III atoms are released by distorting the equilateral triangles to isosceles triangles. Beyond a critical volume, magnetic moments on the Mn IV develop and a weak distortion of the crystalline structure occurs as the spin canting relieves the magnetic frustration.

To conclude, the crystal structure of α-Mn is essentially a consequence of these conflicting tendencies. The noncollinear magnetic structure is due to the fact that the Mn IV atoms arranged on triangular faces are not entirely NM - their frustrated AFM coupling leads to the formation of a local spin structure reminiscent of the Neél structure of a frustrated triangular antiferromagnet. Consequently, the other magnetic moments are rotated out of their collinear orientation. The calculated crystalline and magnetic structures are in good agreement with experiment. However, it is suggested that the magnetism leads to a splitting of the crystallographically inequivalent sites into a larger number of magnetic subgroups than that deduced from the magnetic neutron diffraction, but in accordance with NMR experiments.

3.3 Geometric Frustration in β-Mn

Finally, we briefly review the properties of the remaining four polymorphs of Mn [10]. At 1000 K, a structural phase transition to the β phase occurs. β-Mn is simple cubic with 20 atoms in the unit cell. In the high-temperature state, where it is stable, it is paramagnetic. The face-centered cubic (fcc) γ-phase is stable in the narrow temperature interval between 1368 and 1406 K. At higher temperatures up to the melting point of 1517 K the δ-phase has a body-centered cubic (bcc) structure. γ-Mn quenched to room temperature is face-centered tetragonal; the small tetragonal distortion ~0.17% is caused, similar to the distortion of the α-phase, by AFM ordering. At high pressure a structural phase transition to the ε-phase occurs, which has a hexagonal structure.

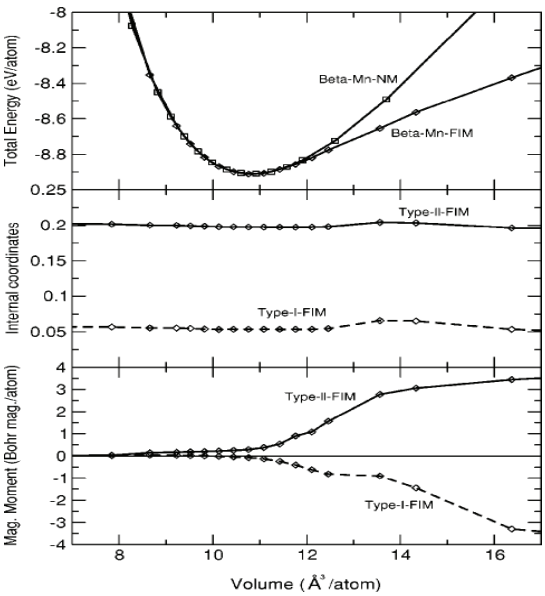

Figure 7 : Total energy, internal structural parameters and local ferrimagnetic moments for β-Mn.

Frustration of the AFM exchange interaction (which is the driving force leading to noncollinearity in α-Mn) is found to be even stronger in β-Mn. However, in contrast to the current assumption that the magnetic frustration is restricted to the sublattice of the Mn II atoms, with the Mn I atoms remaining NM, these studies showed that the AFM Mn I - Mn II coupling is strongest, leading to the stabilization of a FM phase upon slight expansion. At equilibrium, a NM and a weakly ferrimagnetic phase are energetically virtually degenerate. Our results for the total energy, internal structural parameters, and magnetic moments of β-Mn are summarized in Figure 7. At all atomic volumes lower than about 11.8 Å, a NM and an almost ferrimagnetic β-Mn are energetically degenerate within the accuracy of our calculations, which is a few meV/atom. At expanded volumes, a ferrimagnetic state with large moments exist on Mn II sites and smaller, but by no means negligible, moments on Mn I sites. We have also made attempts to find a noncollinear spin configuration, but the calculations always relaxed to a NM or to a nearly collinear ferrimagnetic state, depending on volume. AFM ground states are also found for face-centered γ-Mn and body-centered δ-Mn, while hexagonal ε-Mn is only marginally magnetic at equilibrium. In summary, magnetism strongly influences the mechanical properties of all polymorphs. The structural and magnetic phase diagram of even the complex metallic element Mn is well explained by the density-functional theory.

4 CONCLUSIONS

In this paper we have shown how the PAW method is used to calculate the noncollinear magnetic structures of materials. The magnetization density is treated as a continuous vector variable of position. The approach allows the atomic and magnetic structures to relax simultaneously and self-consistently. Applications have ranged from small Fe and Cr clusters to triangular Cr and Mn monolayers and overlayers on Cu substrates. Finally, we investigated the interesting magnetic properties of the complex metallic element Mn. Magnetization density is observed to vary smoothly with position. The spin direction only changes at the Bloch wall between atoms where the charge and magnetization densities are small, and not due to a rotation of the magnetization. These conclusions support the widely used approximation of a single spin direction for each atomic sphere.

5 ACKNOWLEDGEMENTS

We gratefully acknowledge financial support from EU programs through contract No's CHRXCT93-0337, ERBCHBICT930756 and ERBFMRXCT980178.

6 REFERENCES

[1] T. Oda, A. Pasquarello, and R. Car, Phys. Rev. Lett., 80, 3622, (1998)
[2] O. Ivanov, and V.P. Antropov, J. Appl. Phys., 85, 4821, (1999)
[3] L. Nordström, and D.J. Singh, Phys. Rev. Lett., 76, 4420, (1996)
[4] T. Asada, G. Bihlmayer, S. Handschuh, S. Heinze, Ph. Kurz, and S.Blügel, J. Phys.: Condens. Matter 11, 9347 (1999)
[5] U. von Barth and L. Hedin, J. Phys. C: Solid State Phys. 5, 1629 (1972).
[6] J. Kübler, K. H. Höck, and J. Sticht, J. Appl. Phys. 63, 3482 (1988).
[7] D. Hobbs, G. Kresse, and J. Hafner, Phys. Rev. B, 62, 11556-11569, (2001)
[8] D. Hobbs, and J. Hafner, J. Phy.: Condens. Matter, 12, 7025-7040, (2000)
[9] D. Hobbs, J. Hafner, and D. Spišák, Phys. Rev. B, 68, 014407, (2003)
[10] J. Hafner, and D. Hobbs, Phys. Rev. B, 68, 014408, (2003)